Title

The AFB1 auxin receptor controls the cytoplasmic auxin response pathway in Arabidopsis thaliana.

Journal

Zhi wu sheng li xue bao = Acta phytophysiologica Sinica / Zhongguo zhi wu sheng li xue hui zhu bian, 16(7)

Authors

Dubey, Shiv

Han, Soeun

Stutzman, Nathan

et al.

Publication Date

2023-07-03

DOI

10.1016/j.molp.2023.06.008

Peer reviewed

HHS Public Access

Author manuscript

Mol Plant. Author manuscript; available in PMC 2024 July 03.

Published in final edited form as:

Mol Plant. 2023 July 03; 16(7): 1120–1130. doi:10.1016/j.molp.2023.06.008.

The AFB1 auxin receptor controls the cytoplasmic auxin response pathway in *Arabidopsis thaliana*

Shiv Mani Dubey[1,#], **Soeun Han**[2,#], **Nathan Stutzman**[2], **Michael J Prigge**[2], **Eva Medvecká**[1], **Matthieu Pierre Platre**[3], **Wolfgang Busch**[3], **Matyáš Fendrych**[1,*], **Mark Estelle**[2,*]

[1]Department of Experimental Plant Biology, Faculty of Sciences, Charles University, Prague, Czech Republic

[2]Section of Cell and Developmental Biology, University of California San Diego, La Jolla, United States

[3]Plant Molecular and Cellular Biology Laboratory and Integrative Biology Laboratory, Salk Institute for Biological Studies, La Jolla, United States

Abstract

The phytohormone auxin triggers root growth inhibition within seconds via a non-transcriptional pathway. Among members of the TIR1/AFBs auxin receptor family, AFB1 has a primary role in this rapid response. However, the unique features that confer this specific function have not been identified. Here we show that the N-terminal region of AFB1, including the F-box domain and residues that contribute to auxin binding, are essential and sufficient for its specific role in the rapid response. Substitution of the N-terminal region of AFB1 with that of TIR1 disrupts its distinct cytoplasm-enriched localization and activity in rapid root growth inhibition. Importantly, the N-terminal region of AFB1 is indispensable for auxin-triggered calcium influx which is a prerequisite for rapid root growth inhibition. Furthermore, AFB1 negatively regulates lateral root formation and transcription of auxin-induced genes, suggesting that it plays an inhibitory role in canonical auxin signaling. These results suggest that AFB1 may buffer the transcriptional auxin response while it regulates rapid changes in cell growth that contribute to root gravitropism.

Short Summary

The phytohormone auxin triggers ultra rapid responses in Arabidopsis roots, such as a cytoplasmic calcium spike, enabling rapid gravitropic response of roots. The AFB1 auxin receptor controls these early auxin responses from the cytoplasm of root cells, and in addition negatively regulates the emergence of lateral roots.

[*]For correspondence: matyas.fendrych@natur.cuni.cz and mestelle@ucsd.edu.

[#]These authors contributed equally, the order of the first authors was decided by flipping a coin

Author Contributions

SH and SMD performed most of the experiments and analyzed the data. MF and ME initiated the study. NS, MJP, EM, and MPP performed experiments. SH and SMD drafted the manuscript and prepared the figures, MF, ME and WB edited the manuscript.

Keywords

Gravitropism; calcium; auxin signaling; Arabidopsis; lateral root

Introduction

The plant hormone auxin has a complex role in diverse aspects of plant growth and development. Recent studies have demonstrated that this complexity is related to the existence of multiple auxin-signaling pathways (Weijers and Wagner, 2016; Dubey et al., 2021; Ang and Østergaard, 2023). The best characterized of these is the nuclear signaling pathway, known to regulate the transcription of thousands of genes in a context-specific manner. In the absence of auxin, the AUXIN/INDOLE ACETIC ACID (Aux/IAA) transcriptional repressors bind to the AUXIN RESPONSE FACTOR (ARF) transcription factors and inhibit transcription. Auxin acts by stabilizing the interaction between the TRANSPORT INHIBITOR RESPONSE1 (TIR1)/AUXIN-SIGNALING F-BOX (AFB) proteins and the Aux/IAA proteins, leading to their ubiquitylation and degradation by the proteasome. Once the Aux/IAAs are removed, the ARFs are free to activate transcription of downstream genes (Weijers and Wagner, 2016). In Arabidopsis, TIR1/AFB F-box auxin receptor family consists of six members with largely overlapping roles (Prigge et al., 2020). Apart from TIR1/AFB-dependent regulation, auxin also binds directly to the ETTIN/ARF3 protein and regulates its transcriptional activity (Simonini et al., 2016).

In addition to changes in gene transcription, non-transcriptional responses to auxin have been described (reviewed in Dubey et al., 2021). Several of these rapid responses involve the TRANSMEMBRANE KINASE (TMK) family of receptor-like kinases. The TMKs, possibly in association with the auxin receptor AUXIN BINDING PROTEIN 1 (ABP1), mediate activation of ROPs (Rho-like GTPase from plants) and their downstream effectors such as the cytoskeleton or vesicle trafficking. Recently, the ABP1-TMK module has been shown to be required for very rapid changes in protein phosphorylation in Arabidopsis seedlings. Overall, changes in the phosphoproteome are important for activation of H^+-ATPases and vascular regeneration, among other processes (Friml et al., 2022).

A hallmark of non-transcriptional responses is the near-instantaneous inhibition of root elongation in response to auxin (Monshausen et al., 2011; Fendrych et al., 2018). This response was first described several decades ago (Evans et al., 1994) and later shown to require the putative Ca^{2+} channel CYCLIC NUCLEOTIDE GATED CHANNEL 14 (CNGC14) (Shih et al., 2015). Indeed, the rapid root growth response is associated with very rapid Ca^{2+} influx into the cytoplasm, apoplastic alkalization, and membrane depolarization (Monshausen et al., 2011; Shih et al., 2015; Dindas et al., 2018; Serre et al., 2021; Li et al., 2021). Surprisingly, the rapid response of roots was shown to be dependent on AFB1, a member of the TIR1/AFB auxin receptor family previously only associated with the transcriptional response (Fendrych et al., 2018; Prigge et al., 2020; Serre et al., 2021). Further, the loss of AFB1 alone was sufficient to result in a significant defect in rapid root growth inhibition (Prigge et al., 2020; Serre et al., 2021), indicating its dominant role in this process. Physiological and genetic studies revealed that the rapid auxin response and AFB1

were important for root gravitropism (Shih et al., 2015; Serre et al., 2021). Intriguingly, AFB1 was previously reported as a non-canonical F-box protein since it contains natural polymorphism in the F-box region, which decreases its interaction with CULLIN1 (CUL1), leading to inefficient assembly into the SCF complex (SKP-Cullin-F-box) (Yu et al., 2015). In addition, AFB1 showed a conspicuous cytoplasmic localization (Prigge et al., 2020). These results indicate that AFB1 may possess distinct molecular features, which contribute to its functional specificity for the rapid root growth inhibition by auxin.

In this study, we demonstrate that AFB1 functions in the cytoplasm and is required for rapid Ca^{2+} influx in response to auxin. Further, we show that the AFB1 F-box domain determines its cytoplasmic localization and that a region just adjacent to the F-box is required for AFB1-specific activity in the rapid response. Finally, we document complex interactions between the rapid cytoplasmic auxin response and the nuclear transcriptional pathway.

Results and Discussion

AFB1 triggers auxin-dependent Ca^{2+} influx

Consistent with previous results, we confirmed that the *afb1* mutant is resistant to auxin during the first 20 minutes of treatment whereas the *tir1* mutant is similar to wild type (Fig. S1A). As time progressed, the level of resistance in the *afb1* mutant decreased while resistance of the *tir1* mutant increased (Fig. 1A). This behavior is consistent with the roles of AFB1 and TIR1 in the nongenomic and transcriptional response, respectively. To test the role of receptors other than AFB1 in the rapid response, we measured auxin-induced root growth inhibition and the dynamics of the gravitropic response in the *tir1afb2* and *tir1afb345* mutants. Both the mutants responded to IAA similarly to wild type (Fig. 1B). Previously, the *tir1afb345* mutant was shown to be auxin resistant during the first 20 minutes after treatment (Prigge et al., 2020). The basis for this difference is unknown but it might be related to the highly variable phenotype of *tir1afb345* seedlings (Prigge et al., 2020). Consistent with root growth inhibition, the *afb1* mutant showed a delay in early gravitropic response, however *tir1afb2* and *tir1afb345* mutants responded with a similar dynamics to the Col-0 control (Fig. 1C; Supp. movie 1).

To exert greater control of the rapid auxin response, we prepared *Arabidopsis thaliana* lines expressing fluorescent protein-tagged versions of the synthetic receptor-ligand system – ccvTIR1 and ccvAFB1 controlled by the *pTIR1* promoter. The ccv (concave) receptor versions are ‘blind’ to the natural auxin IAA. Instead, they bind the synthetic cvxIAA (convex IAA, Uchida et al., 2018) (Fig. 1D,E), and show similar subcellular localization to the native proteins (Fig. 1F). The ccvAFB1 protein was sufficient to trigger rapid root growth inhibition when seedlings were treated with cvxIAA (Fig. 1G). In previous studies it was shown that the cvxIAA-ccvTIR1 pair triggers a response that is several minutes delayed in comparison to the effect of natural IAA (Fendrych et al., 2018; Li et al., 2021). In our experiments, the cvxIAA – ccvTIR1 pair triggers a response that is significantly slower (Serre et al., 2021) than the cvxIAA – ccvAFB1 system. Taken together, these results clarify previous discrepancies regarding the overlapping function of F-box receptors in the context of rapid auxin responses and suggest that AFB1 is the primary receptor for the rapid auxin responses.

One of the earliest detectable responses to auxin in the root is the influx of calcium (Ca^{2+}) (Monshausen et al., 2011). A mutant lacking the CNGC14 calcium channel shows a delay in the gravitropic response(Shih et al., 2015) that resembles the *afb1* gravitropic defect (Serre et al., 2021), hinting at a role for AFB1 in auxin-dependent Ca^{2+} influx. We therefore visualized cytosolic Ca^{2+} levels in the *afb1* mutant using the R-GECO1 sensor (Keinath et al., 2015) and vertical microscopy coupled to microfluidic imaging chips (Serre et al., 2021). The control line showed an almost immediate elevation in cytosolic Ca^{2+} (calcium transient) in response to 150 nM IAA, as described before (Shih et al., 2015; Dindas et al., 2018; Wang et al., 2022). Strikingly, in *afb1* roots, cytosolic Ca^{2+} did not increase after auxin application; instead, a mild Ca^{2+} increase occurred only ca. 240 seconds after the treatment (Fig. 1H,I, Supp. movie 2). This indicates that the AFB1 receptor is required for the auxin-induced Ca^{2+} transient.

To test whether AFB1 is upstream and sufficient for the Ca^{2+} transient, we introduced the RGECO-1 sensor into the *ccvAFB1* and *ccvTIR1* lines. While in both the control and the *ccvTIR1* line, the application of 500 nM cvxIAA did not elicit a detectable Ca^{2+} transient, the compound triggered an immediate Ca^{2+} transient in the *ccvAFB1* line (Fig. 1J, Supp. movie 3). In contrast to these results, cvxIAA has been reported to trigger a Ca^{2+} spike in a ccvTIR1 line expressing the GCaMP3 sensor (Qi et al., 2022). We speculate that cvxIAA might trigger a transient detectable by GCAMP. However, the difference between control, ccvTIR1 and ccvAFB1 R-GECO-1 lines indicates that ccvAFB1 is required and sufficient for cytosolic Ca^{2+} increase (Fig. 1J).

Finally, to determine if AFB1 is sufficient to trigger Ca^{2+} influx in the case of the native receptor, we analyzed IAA-induced Ca^{2+} transient in the *tir1afb345* and *tir1afb2* mutants. Unfortunately, the RGECO-1 construct was silenced in the *tir1afb345* line. On the other hand, the *tir1afb2* mutant responded to IAA treatment with a Ca^{2+} transient comparable to the wild-type control (Fig. 1K, Supp. movie 4). These results show that AFB1 is upstream of the auxin-induced Ca^{2+} transient that triggers the rapid growth responses including early root gravitropic responses (Shih et al., 2015; Dindas et al., 2018; Serre et al., 2021). Whether or not AFB1 acts through CNGC14 remains uncertain. The *afb1*, *cngc14* and *afb1/cngc14* double mutant lines all showed identical defects in rapid auxin response hinting that the two proteins function in the same pathway (Fig.S1B). In contrast, AFB1 overexpression resulted in a tendency to increase rapid auxin response in the *afb1/cngc14* double mutant background (Fig.S1B). Although this increase was not statistically significant, it does suggest that AFB1 can also act independently of CNGC14, possibly recruiting other CNGC paralogs in the roots when AFB1 is overexpressed.

It is intriguing that AFB1 has recently be shown to have adenyl cyclase (AC) activity (Qi et al., 2022). Thus, it is possible that AFB1-mediated cAMP production in the cytoplasm triggers the activity of the CNGC14 channel. On the other hand, TIR1 has also been shown to have AC activity and our data clearly demonstrate that this protein does not function in the rapid response, even when it is in the cytoplasm. Thus the relationship between CNGC4, AFB1, and its AC activity awaits further investigation.

AFB1 triggers rapid auxin response from the cytoplasm

Despite the apparent differences in their modes of action, TIR1 and AFB1 are the most recently diverged members of the TIR1/AFB family in *Arabidopsis* (Prigge et al., 2020). To determine if their functional specificity is related to their expression pattern, we expressed TIR1 in the *AFB1* expression domain. The *pAFB1:TIR1-mCitrine* expression pattern mimicked the AFB1 expression pattern (Prigge et al., 2020) (Fig. S1C). However, the transgene failed to rescue the *afb1* phenotype (Fig. S1D) even though the levels of AFB1 and TIR1 proteins were similar in these lines (Fig. S1C). As expected, the *pAFB1:AFB1-mCitrine* transgene *(gAFB1* #1 and *gAFB1* #2*)* complemented the *afb1* phenotype. Interestingly, one of the *AFB1* complementation lines, *gAFB1 #2*, exhibited a higher expression level than either the wild-type or *gAFB1 #1* (Fig. S1E,F) and showed a hypersensitive rapid response to auxin (Fig. S1G). These data suggest that the functional differences between TIR1 and AFB1 are related to differences in their protein sequences, rather than expression pattern.

We previously showed that the TIR1/AFB proteins are partitioned between the cytoplasm and the nucleus. Interestingly, AFB1 is both the most abundant member of the family and highly enriched in the cytoplasm, while TIR1 is primarily nuclear (Prigge et al., 2020). To determine if subcellular localization is decisive for function in the rapid response, we added either a NUCLEAR LOCALIZATION SEQUENCE (NLS) or NUCLEAR EXCLUSION SEQUENCE (NES) to the AFB1-mCitrine receptor (*gAFB1-NLS* and *gAFB1-NES*). The resulting fusion proteins were highly enriched in the nucleus and cytoplasm respectively as expected (Fig. 2A). Intriguingly, only AFB1-NES rescued the phenotype of *afb1* (Fig. 2B), demonstrating that AFB1 must be localized to the cytoplasm to mediate rapid root growth inhibition. In a complementary approach, we attempted to generate *gTIR1-NES-mCitrine* plants but failed to recover lines with significant levels of TIR1 accumulation despite the presence of high transcript levels (Fig. S1H,I). It is possible that TIR1 is particularly unstable in the cytoplasm.

It has been reported that a polymorphism within the F-box domain of AFB1 (K at position 8 rather than E) strongly reduces its ability to interact with CUL1 and assemble into an SCF complex (Yu et al., 2015). The TIR1 E12K mutation, recapitulating AFB1, significantly reduces the interaction with CUL1 and results in a strong auxin-resistant phenotype (Yu et al., 2015). To test whether the differential affinity of TIR1 and AFB1 for CUL1 determines their distinct subcellular localization and function, we prepared the E12K version of ccvTIR1 to mimic the weak binding affinity of AFB1 with CUL1. Surprisingly, the protein still localized to the nucleus (Fig. 2C), interacted with the degron domain of Aux/IAA7 in a cvxIAA-dependent manner *in vitro* (Fig. S2A), but was unable to inhibit root growth in response to cvxIAA (Fig. 2D). We also expressed TIR1 E12K and AFB1 K8E in Arabidopsis protoplasts; these amino acid substitutions did not impact cellular localization (Fig. 2E). These results indicate that the association with the SCF complex is not required for the co-receptor assembly and does not determine cellular localization.

As AFB1 does not bind CUL1 efficiently, we tested the possibility that AFB1 functions independently of an SCF complex by examining the rapid auxin response in the *cul1–6* and *cul1–7* mutants. *CUL1* is an essential gene during embryogenesis but these two

hypomorphic alleles are viable and auxin resistant in a long-term root growth assay (Moon et al., 2007; Gilkerson et al., 2009). Both the *cul1–6* and *cul1–7* mutants exhibited a normal rapid response (Fig. 2F). In addition, AFB1 localization was not altered in the *cul1–6* mutant, confirming that AFB1 localization is not regulated by interaction with CUL1 (Fig. 2G). Similarly, recently published proteomic data(Li et al., 2021) confirms that TIR1, but not AFB1, interact with CUL1 in an IP-MS experiment, despite the relative abundance of AFB1. In contrast, both TIR1 and AFB1 interact with ASK1 as expected since this had been shown previously (Yu et al., 2015). These results suggest that CUL1 binding and presumably SCF complex formation are not required for AFB1-triggered rapid root growth inhibition.

The well-known substrates for $SCF^{TIR1/AFB}$ are the Aux/IAA transcriptional repressors. AFB1 has been shown to interact with several members of this family, either in Y2H assays or in plants (Calderón Villalobos et al., 2012). We tested the *axr2–1* and *shy2–2* mutants in the rapid response assay. These two lines have mutations in the DII region of IAA7 and IAA3 respectively, that act to stabilize the protein and confer auxin resistance in long term root growth assays (Tian and Reed, 1999; Nagpal et al., 2000). Neither mutant exhibited a significant change in rapid root growth inhibition (Fig. S1J), suggesting that Aux/IAA proteins do not contribute to the rapid response. Although these results suggest that the Aux/IAAs may not be involved in the rapid response, it is important to note that there are 28 members in the family and it is possible that one or more of these have specialized function in the cytoplasm.

The F-box domain determines the subcellular localization of the AFB1 and TIR1 receptors

To identify the domains responsible for AFB1-specific localization and function, we generated a set of *TIR1/AFB1* domain swap constructs under control of the *AFB1* promoter and introduced them into the *afb1* mutant. The chimeric proteins are named according to the origin of each segment; T for TIR1, and A for AFB1 (Fig. 3A). As shown earlier, AFB1 (or AAAA) was localized to both nucleus and cytoplasm, and rescued the *afb1* phenotype, while TIR1 (TTTT), was largely localized to the nucleus and failed to restore the *afb1* defect (Fig. 3B,C). Interestingly, among the 4 chimeric proteins, only TAAA was abundant in the nucleus similar to TIR1, and failed to restore the *afb1* mutant sensitivity to auxin. The ATAA, AATA, and AAAT chimeric proteins localized to both the nucleus and cytoplasm (Fig. 3B) and restored auxin sensitivity to the mutant (Fig. 3C). These results indicate that the N-terminal segment of AFB1 is important for AFB1's cytoplasmic localization and function and that this region determines the nucleus/cytoplasm ratio of the protein (Fig. 3D, Fig. S2B). This region includes the F-box domain that mediates the interaction between F-box proteins, ASK proteins and CUL1, and the N-terminal part of the Leucine-rich repeat domains (LRR) that participates in auxin and/or Aux/IAA binding (Tan et al., 2007; Calderón Villalobos et al., 2012) (Fig. 3A). We therefore created two additional chimeric proteins. One contained the entire region 1 (iATTT) while the second contained only the F-box from AFB1 (fbATTT) (Fig. 3A) and expressed them under the control of *pAFB1* and *pTIR1* promoters, respectively. Note that both *pTIR1* and *pAFB1* are active in the epidermis (Prigge et al., 2020) and iATTT and fbATTT are both localized to nucleus and cytoplasm (Fig. 3E). However, only iATTT rescued the *afb1* phenotype (Fig. 3F), and elicited a Ca^{2+} transient similar to that of wild-type (Fig. 3G,H; Supp. movie

5). The iATTT showed a patchy expression pattern, and interestingly, we only observed Ca^{2+} transients in iATTT expressing cells demonstrating the cell-autonomous nature of the auxin-triggered Ca^{2+} transient. To corroborate the results, we created the ccv-fbATTT version of the receptor, which also showed cytoplasmic and nuclear localization (Fig. S2C), and interacted with the degron domain of Aux/IAA7 in a cvxIAA-dependent manner *in vitro* (Fig. S2A). However, like fbATTT, ccv-fbATTT failed to trigger root growth inhibition in response to cvxIAA (Fig. S2D). Finally, consistent with the previous results, the fbATTT line failed to restore the early gravitropic response of *afb1* mutant, while iATTT almost completely recovered the response (Fig. 3I, Supp.movie6). The lack of full complementation can be explained by the patchy expression of iATTT in the root tip (Fig. 3G).

These results indicate that the F-box domain determines the cytoplasmic/nuclear partitioning of the receptors; that the cytoplasmic localization of the auxin receptor is required but not sufficient for function in the rapid response; and, finally, that the sequences in the N-terminal part of the AFB1 LRR domain are required for the function in the rapid auxin response. Since bioinformatic analysis did not reveal a clear nuclear-localization signals (NLS) or nuclear exclusion signal (NES) in the F-box domains of TIR1 or AFB1, it is possible that an unknown protein interacting with the F-box domain is involved in the regulation of subcellular localization.

AFB1 signaling negatively regulates the nuclear auxin response

Since AFB1 is abundant in both the cytoplasm and nucleus, we also determined the effects of manipulating AFB1 levels on long term auxin responses that are mediated by canonical auxin signaling. In a long-term root growth assay, we found that the *gAFB1-NLS* line displayed significant auxin resistance, while the *gAFB1-NES* line was slightly hypersensitive (Fig. 4A, S3A). Auxin-hypersensitivity of the line expressing AFB1-NES suggests that the rapid AFB1-dependent pathway can also affect auxin response over a longer time frame. However, we could not exclude the possibility that cytoplasmic AFB1 also negatively affects canonical auxin signaling because this effect could be masked by the AFB1-mediated root growth inhibition.

Earlier genetic studies suggested that AFB1 may be a negative regulator of LR formation (Prigge et al., 2020). Here we show that the *afb1* mutant produces slightly more lateral roots than wild type while two AFB1 complementation lines (*gAFB1 #1* and *#2*), which accumulate higher levels of AFB1 than the control, produce many fewer lateral roots, confirming this hypothesis (Fig. 4B,C). Interestingly, the lines expressing AFB1-NLS and AFB1-NES also have reduced numbers of LR (Fig. 4B,C). All three lines, *gAFB1, gAFB1-NLS* and *gAFB1-NES*, exhibited significantly increased numbers of early stage LR (stages I-II) (Fig. 4D) compared to wild type indicating that AFB1 does not affect LR initiation, but rather suppresses LR emergence, when it is present in either the cytoplasm or nucleus. In addition, we observed that all three AFB1 proteins, AFB1, AFB1-NLS and AFB1-NES are broadly expressed in both developing primordia and its overlaying tissues (Fig. 4E, S3A).

To determine if the role of AFB1 during lateral root development is associated with auxin regulated transcription we examined the expression of the auxin-responsive genes *IAA5, IAA6, IAA19* and two lateral root-related genes, *LBD16* and *LBD29* (Okushima et al.,

2007). As expected, auxin treatment increased expression of these genes in wild-type seedlings (Fig. S3B). Intriguingly, induction of *IAA5, IAA6* and *LBD29* was greater in *afb1*, but suppressed in a dose-dependent fashion in the *AFB1* complementation lines (*gAFB1#1* and *gAFB1#2*). Moreover, this suppression was also observed in *gAFB1-NLS* (Fig. S3B). These results are consistent with the lateral root phenotype of these lines. Surprisingly, auxin induction of gene expression was also suppressed in *gAFB1-NES* seedlings. These data indicate that both nuclear and cytoplasmic AFB1 function as a negative regulator of auxin-mediated transcription, presumably leading to the inhibition of canonical auxin signaling during long-term development.

Taken together, we propose that while cytoplasmic AFB1 induces non-genomic rapid auxin response which is dependent on CNGC14-mediated Ca^{2+} signaling, both nuclear and cytoplasmic AFB1 inhibit canonical auxin signaling. In the case of nuclear AFB1, the protein may act as a dominant-negative in a manner similar to TIR1(E12K) (Yu et al., 2015). In contrast, how cytoplasmic AFB1 acts to suppress the canonical pathway is unknown. Regardless, this activity may serve to integrate the two auxin responses as the root responds to changing environmental conditions.

Materials and Methods

Plant Materials and growth conditions

All *Arabidopsis* mutants in this study were Col-0 background. The *afb1–3*, *tir1–1*, *tir1–1 afb1–3*, *tir1afb2*, *tir1 afb345,* and *gAFB1-mCitrine* (*afb1–3*) were used previously (Prigge et al., 2020), the *cngc14* line is the SALK_206460 (Shih et al., 2015). The *shy2–2*, *axr2–1*, *cul1–6,* and *cul1–7* were previously described (Tian and Reed, 1999; Nagpal et al., 2000; Moon et al., 2007; Gilkerson et al., 2009). Transgenic lines used are listed in Supplementary table 1. The R-GECO1 Ca^{2+} sensor was introduced by crossing or transformation into the respective mutants. Seeds were sterilized with bleach (3% NaClO) and stratified in the dark cold room for 2–4 days. Plants were vertically grown on ½ MS media containing 0.8–1.0% agar, 1% (w/v) sucrose, adjusted to pH 5.8 with KOH, and kept at 22 °C in a long day(16L/8D), growth room maintaining 60% humidity, and a light intensity of 100 μmol photons m^{-2} s^{-1}.

Molecular cloning

TIR1(AT3G62980) domains were inserted into corresponding PCR-amplified *pMiniT-gAFB1(AT4G03190)* backbone fragments(Prigge et al., 2020) using the NEBuilder HiFi DNA assembly kit (NEB). For generating *NLS/NES* tagged lines, *NLS/NES-mCitrine* fragment was inserted into *pMiniT-gAFB1/TIR1* constructs (Prigge et al., 2020). These *pMiniT-gAFB1/gTIR1-mCitrine* were subcloned into the *pMP535* binary vector as described previously. The first 53 and 57 amino acids of AFB1 and TIR1, respectively, ending in CYAVS were used to generate the *fbATTT* construct. The *ccvTIR1* and *ccvAFB1/ccvfb-ATTT* lines were generated by the substitution mutations F79>G in TIR1 (Uchida et al., 2018) and F75>G in AFB1 respectively. The ccvTIR1 E12K mutation was created as described before (Yu et al., 2015). The *ccvTIR1*, *ccvAFB1*, *ccvfb-ATTT*, *fbATTT*, and *ccvTIR1 E12K* fragments were assembled with *TIR1* promoter, *mScarlet-I* (Bindels et al.,

2017) or *mVenus* tag, and 35s terminator and then moved into the *pDGB3omega1* binary vector using GoldenBraid method (Sarrion-Perdigones et al., 2013). The transgenic lines used in the study are summarized in Supplementary Table 1; all primers used for cloning are listed in Supplementary Table 2.

Root growth assay

Rapid root growth inhibition assay was performed by two methods. In first method, five-day-old seedlings were transferred to culture chambers containing the growth medium supplemented with 0 or 10 nM IAA, and immediately imaged every 25 sec for 20 min or every 72 sec for 1 hr. The 50 images taken for 20 min or 1 hr were processed to generate growth curve by MATLAB software using a customized MATLAB script (Prigge et al., 2020; Platre, 2022). In the second method, seedlings were transferred to growth medium containing either 0 or 10 nM IAA, and immediately transferred to a 3D-printed microscopy chamber and placed on the vertical microscope. Roots were imaged for 10 minutes after each 5 min. Root growth (length increment) measured after stabilizing the background drift of the root tip using the Fiji plugin correct 3D drift. For measuring long-term root growth, seedlings were imaged at 1,200 dpi using a flatbed scanner at 0, 3hr and 6hr after transferring onto treatment medium (0 and 10 nM IAA). Root tips of individual seedlings were marked at each time point, and root growth increment was measured using the segmented line tool in FIJI. The root growth response to auxin was calculated as the length increment in treatment divided by the length increment in control conditions. The response value 1 indicates that the treatment did not affect root growth.

Quantification of gravitropic response

Thin layer of growth medium containing five-day-old seedlings was placed into a 3D-printed microscopy chamber. The chamber was placed vertically on the vertical stage microscope for 45 minutes to recover. Then the chamber was rotated by 90 degrees. After the 2 min needed to set the imaging, the roots were imaged every minute for 43 minutes. The root tip angles were measured using ACORBA v1.2 as described (Serre and Fendrych, 2022).

Pull down and western blotting

Pulldowns were done as previously described (Kepinski, 2009) with modification. Briefly, seven-day-old seedlings were used for total protein extraction using extraction buffer. The biotinylated Aux/IAA7 DII peptide (AKAQVVGWPPVRNYRKN) was bound to streptavidin-agarose beads. These DII-beads were combined with total protein extract containing either 0 or 10 μM cvxIAA or 10 μM IAA. The reaction was kept at 4 °C for 1 h and then washed 3 times with extraction buffer. Washed pull-down samples were subjected to western blotting. Full images of immunoblotted membranes shown in Fig S4.

Microscopy imaging

Seedlings were stained with a propidium iodide (PI) and mounted on a glass slide for imaging. PI (Ex/Em; 561/642nm), mCitrine (Ex/Em; 514/556nm) and mCherry and mScarletI (Ex/Em;594/628nm) signal were detected using a 20x/0.8 NA air or 40x/1.2 NA WI objective lens on a Zeiss LSM 880, PI and mScarletI signals were distinguished

by linear unmixing. For imaging fluorescence signal in *Arabidopsis* protoplast, constructs under *CaMV35S promoter* were transfected into Col-0 protoplast (Yoo et al., 2007; Han, 2018). Transfected protoplasts were incubated overnight and imaged on glass slides using 20X/0.8 NA air objective (Ex/Em;488/507nm). Relative nuclear localization was calculated as the value of nuclear fluorescence signal divided by whole cell fluorescence signal in each protoplast cell (n=19–20). The fluorescence signal intensity was determined by Area*Mean grey value from each ROI to mark nucleus and whole cell region in FIJI. To determine the cytoplasm/nucleus ratio in roots, we followed the ClearSeeAlpha protocol (Kurihara et al., 2021). The cell walls and nuclei were stained with SCRI Renaissance 2200 and TO-PRO-3 iodide, respectively (Tofanelli et al., 2019), and signal was quantified as described in (Prigge et al., 2020); the fraction on mCitrine signal in the nucleus was calculated as $[Area_{nuc} \times (MeanGray_{nuc} - MeanGray_{bg})] \div [Area_{cell} \times (MeanGray_{cell} - MeanGray_{bg})]$. We imaged the following number of plants for the respective figures: Fig.1F: >10; Fig.2A,C: >10; Fig.2G: 6 cul1, >10 Col0; Fig.3B,E:>10 for each line; Fig.4E: 6; Fig.S1C,E,H:>10; Fig.S2C:>10; Fig.S3A:>6.

Ca^{2+} transients were visualized using the R-GECO1 reporter (Keinath et al., 2015) and imaged using a microfluidic setup combined with a vertical spinning disk microscope (Serre et al., 2021). Briefly, five-day-old seedlings were transferred to a sealable single-layer PDMS silicone chip, and placed on the microscope for 20 min to recover. The seedlings were imaged every 15 sec for first 5 min with control medium (DMSO), and switched to treatment medium (150 nM IAA or 500 nM cvxIAA) for 10 min using 20x/0.8 objective. Constant media flow and switching between control and treatment medium was performed using OBI1 Elveflow software. R-GECO1 time series images and signal intensity were processed and analyzed in Fiji.

Lateral root measurement

Eight-day-old seedlings were incubated in 0.24 N HCl 20% methanol at 60 °C for 10 minutes, and transferred to 7% NaOH, 7% hydroxylamine-HCl in 60% ethanol for 15 minutes at room temperature. The solution was replaced with a series of 40%, 20% and 10% ethanol for 5 minutes, and stored in 5% ethanol/ 25% glycerol solution (Malamy and Benfey, 1997). The root samples were mounted in 50% glycerol on glass slides and observed in bright field using a 40x/ 1.2 NA WI objective with a DIC filter on a Zeiss LSM 880.

Gene expression analysis

Five-day-old seedlings were transferred to agar media containing 0 or 100 nM IAA and incubated in the growth chamber for 2 hr. Seedling pools (about 30 seedlings per genotype) were used for RNA isolation using Qiagen RNeasy Plant Mini kit. 2 μg of RNA was used for RT-PCR using Superscript III RT-kit or Thermo Maxima H-master mix. qRT-PCR was performed using Bio-Rad SsoAdvanced SYBR mix. Primers used for qRT-PCR are listed in Supplementary Table 2.

Supplementary Material

Refer to Web version on PubMed Central for supplementary material.

Acknowledgements

This work was supported by the National Institute of General Medical Sciences (NIGMS) with grants to ME (R35GM141892) and to WB (R01GM127759), and by the European Research Council (grant no. 803048) to MF. MPP was supported by a long-term postdoctoral fellowship (LT000340/2019 L) by the Human Frontier Science Program Organization. The authors thank Melanie Krebs and Karin Schumacher for providing the R-GECO1 plasmid, Nelson BC Serre for experimental guidance.

References

Ang ACH, and Østergaard L (2023). Save your TIRs - more to auxin than meets the eye. New Phytol. 238:971–976. [PubMed: 36721296]

Bindels DS, Haarbosch L, van Weeren L, Postma M, Wiese KE, Mastop M, Aumonier S, Gotthard G, Royant A, Hink MA, et al. (2017). mScarlet: a bright monomeric red fluorescent protein for cellular imaging. Nat. Methods 14:1–12.

Calderón Villalobos LIA, Lee S, De Oliveira C, Ivetac A, Brandt W, Armitage L, Sheard LB, Tan X, Parry G, Mao H, et al. (2012). A combinatorial TIR1/AFB-Aux/IAA co-receptor system for differential sensing of auxin. Nat. Chem. Biol. 8:477–85. [PubMed: 22466420]

Dindas J, Scherzer S, Roelfsema MRG, von Meyer K, Müller HM, Al-Rasheid KAS, Palme K, Dietrich P, Becker D, Bennett MJ, et al. (2018). AUX1-mediated root hair auxin influx governs SCFTIR1/AFB-type Ca2+ signaling. Nat. Commun. 9:1174. [PubMed: 29563504]

Dubey SM, Serre NBC, Oulehlová D, Vittal P, and Fendrych M (2021). No Time for Transcription-Rapid Auxin Responses in Plants. Cold Spring Harb. Perspect. Biol. 13:a039891.

Evans ML, Ishikawa H, and Estelle MA (1994). Responses ofArabidopsis roots to auxin studied with high temporal resolution: Comparison of wild type and auxin-response mutants. Planta 194:215–222.

Fendrych M, Akhmanova M, Merrin J, Glanc M, Hagihara S, Takahashi K, Uchida N, Torii KU, and Friml J (2018). Rapid and reversible root growth inhibition by TIR1 auxin signalling. Nat. plants 4:453–459. [PubMed: 29942048]

Friml J, Gallei M, Gelová Z, Johnson A, Mazur E, Monzer A, Rodriguez L, Roosjen M, Verstraeten I, Živanović BD, et al. (2022). ABP1-TMK auxin perception for global phosphorylation and auxin canalization. Nature 24.

Gilkerson J, Hu J, Brown J, Jones A, Sun T, and Callis J (2009). Isolation and Characterization of cul1–7, a Recessive Allele of CULLIN1 That Disrupts SCF Function at the C Terminus of CUL1 in Arabidopsis thaliana. Genetics 181:945–963. [PubMed: 19114460]

Han H (2018). RNA Interference to Knock Down Gene Expression. Methods Mol. Biol. 1706:293–302. [PubMed: 29423805]

Keinath NF, Waadt R, Brugman R, Schroeder JI, Grossmann G, Schumacher K, and Krebs M (2015). Live Cell Imaging with R-GECO1 Sheds Light on flg22- and Chitin-Induced Transient [Ca(2+)]cyt Patterns in Arabidopsis. Mol. Plant 8:1188–200. [PubMed: 26002145]

Kepinski S (2009). Pull-down assays for plant hormone research. Methods Mol. Biol. 495:61–80. [PubMed: 19085146]

Kurihara D, Mizuta Y, Nagahara S, and Higashiyama T (2021). ClearSeeAlpha: Advanced Optical Clearing for Whole-Plant Imaging. Plant Cell Physiol. 62:1302–1310. [PubMed: 33638989]

Li L, Verstraeten I, Roosjen M, Takahashi K, Rodriguez L, Merrin J, Chen J, Shabala L, Smet W, Ren H, et al. (2021). Cell surface and intracellular auxin signalling for H+ fluxes in root growth. Nature 599:273–277. [PubMed: 34707283]

Malamy JE, and Benfey PN (1997). Organization and cell differentiation in lateral roots of Arabidopsis thaliana. Development 124:33–44. [PubMed: 9006065]

Monshausen GB, Miller ND, Murphy AS, and Gilroy S (2011). Dynamics of auxin-dependent Ca2+ and pH signaling in root growth revealed by integrating high-resolution imaging with automated computer vision-based analysis. Plant J. 65:309–18. [PubMed: 21223394]

Moon J, Zhao Y, Dai X, Zhang W, Gray WM, Huq E, and Estelle M (2007). A new CULLIN 1 mutant has altered responses to hormones and light in Arabidopsis. Plant Physiol. 143:684–96. [PubMed: 17158585]

Nagpal P, Walker LM, Young JC, Sonawala A, Timpte C, Estelle M, and Reed JW (2000). AXR2 Encodes a Member of the Aux/IAA Protein Family. Plant Physiol. 123:563–574. [PubMed: 10859186]

Okushima Y, Fukaki H, Onoda M, Theologis A, and Tasaka M (2007). ARF7 and ARF19 regulate lateral root formation via direct activation of LBD/ASL genes in Arabidopsis. Plant Cell 19:118–30. [PubMed: 17259263]

Platre M (2022). Root Walker: an automated pipeline for large scale quantification of early root growth responses at high spatial and temporal resolution. bioRxiv 2022.11.16.

Prigge MJ, Platre M, Kadakia N, Zhang Y, Greenham K, Szutu W, Pandey BK, Bhosale RA, Bennett MJ, Busch W, et al. (2020). Genetic analysis of the Arabidopsis TIR1/AFB auxin receptors reveals both overlapping and specialized functions. Elife 9:1–28.

Qi L, Kwiatkowski M, Chen H, Hoermayer L, Sinclair S, Zou M, Del Genio CI, Kubeš MF, Napier R, Jaworski K, et al. (2022). Adenylate cyclase activity of TIR1/AFB auxin receptors in plants. Nature 611:133–138. [PubMed: 36289340]

Sarrion-Perdigones A, Vazquez-Vilar M, Palací J, Castelijns B, Forment J, Ziarsolo P, Blanca J, Granell A, and Orzaez D (2013). GoldenBraid 2.0: a comprehensive DNA assembly framework for plant synthetic biology. Plant Physiol. 162:1618–31. [PubMed: 23669743]

Serre NBC, and Fendrych M (2022). ACORBA: Automated workflow to measure Arabidopsis thaliana root tip angle dynamics. Quant. Plant Biol. 3:e9. [PubMed: 37077987]

Serre NBC, Kralík D, Yun P, Slouka Z, Shabala S, and Fendrych M (2021). AFB1 controls rapid auxin signalling through membrane depolarization in Arabidopsis thaliana root. Nat. plants 7:1229–1238. [PubMed: 34282287]

Shih H-W, DePew CL, Miller ND, and Monshausen GB (2015). The Cyclic Nucleotide-Gated Channel CNGC14 Regulates Root Gravitropism in Arabidopsis thaliana. Curr. Biol. 25:3119–25. [PubMed: 26752079]

Simonini S, Deb J, Moubayidin L, Stephenson P, Valluru M, Freire-Rios A, Sorefan K, Weijers D, Friml J, and Østergaard L (2016). A noncanonical auxin-sensing mechanism is required for organ morphogenesis in Arabidopsis. Genes Dev. 30:2286–2296. [PubMed: 27898393]

Tan X, Calderon-Villalobos L. I. a, Sharon M, Zheng C, Robinson CV, Estelle M, and Zheng N (2007). Mechanism of auxin perception by the TIR1 ubiquitin ligase. Nature 446:640–5. [PubMed: 17410169]

Tian Q, and Reed JW (1999). Control of auxin-regulated root development by the Arabidopsis thaliana SHY2/IAA3 gene. Development 126:711–21. [PubMed: 9895319]

Tofanelli R, Vijayan A, Scholz S, and Schneitz K (2019). Protocol for rapid clearing and staining of fixed Arabidopsis ovules for improved imaging by confocal laser scanning microscopy. Plant Methods 15:120. [PubMed: 31673277]

Uchida N, Takahashi K, Iwasaki R, Yamada R, Yoshimura M, Endo TA, Kimura S, Zhang H, Nomoto M, Tada Y, et al. (2018). Chemical hijacking of auxin signaling with an engineered auxin-TIR1 pair. Nat. Chem. Biol. 14:299–305. [PubMed: 29355850]

Wang R, Himschoot E, Grenzi M, Chen J, Safi A, Krebs M, Schumacher K, Nowack MK, Moeder W, Yoshioka K, et al. (2022). Auxin analog-induced Ca2+ signaling is independent of inhibition of endosomal aggregation in Arabidopsis roots. J. Exp. Bot. 73:2308–2319. [PubMed: 35085386]

Weijers D, and Wagner D (2016). Transcriptional Responses to the Auxin Hormone. Annu. Rev. Plant Biol. 67:539–74. [PubMed: 26905654]

Yoo S-D, Cho Y-H, and Sheen J (2007). Arabidopsis mesophyll protoplasts: a versatile cell system for transient gene expression analysis. Nat. Protoc. 2:1565–72. [PubMed: 17585298]

Yu H, Zhang Y, Moss BL, Bargmann BOR, Wang R, Prigge M, Nemhauser JL, and Estelle M (2015). Untethering the TIR1 auxin receptor from the SCF complex increases its stability and inhibits auxin response. Nat. plants 1.

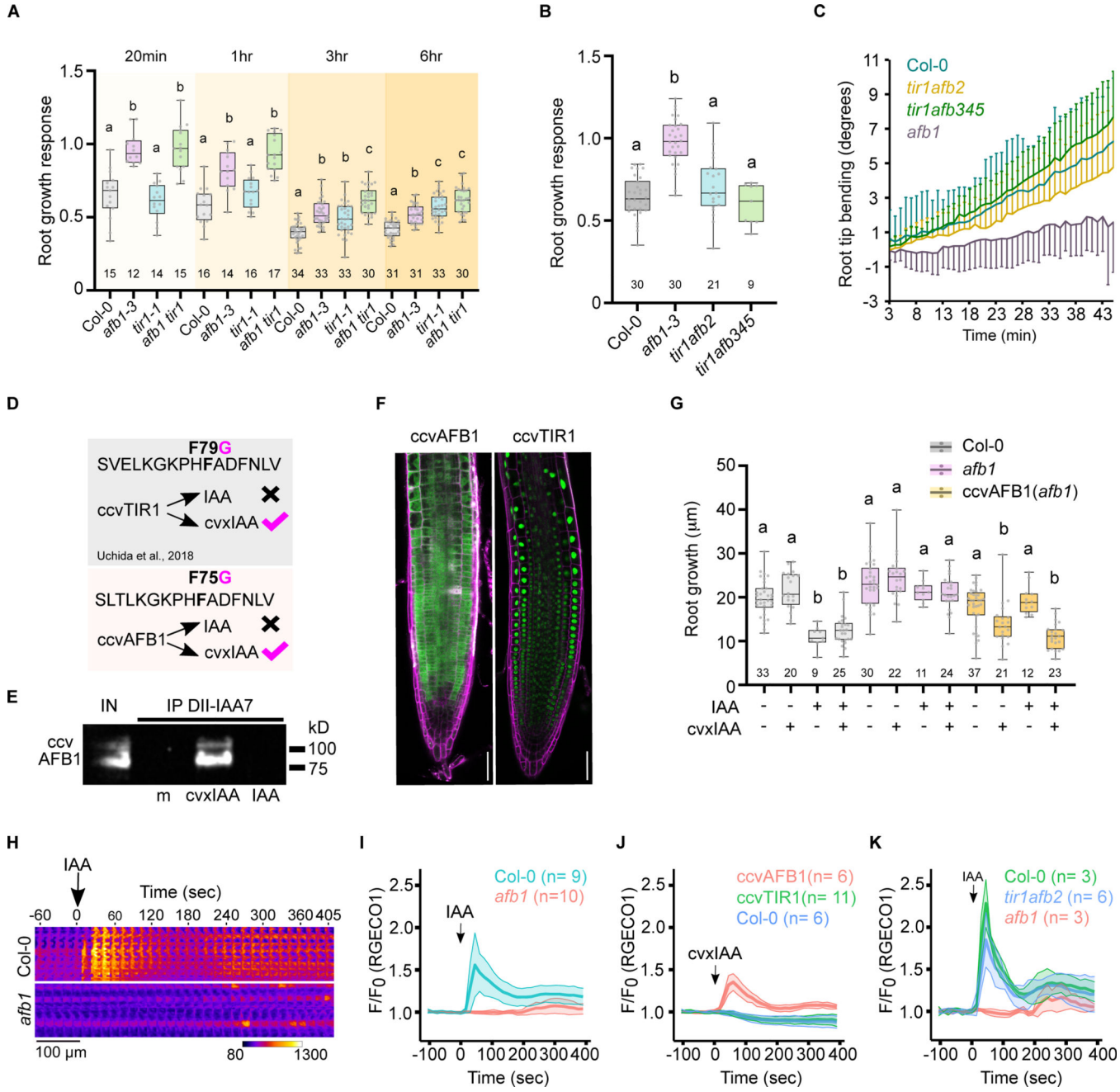

Figure 1: AFB1 triggers auxin-dependent calcium transients and the early phase of root-growth inhibition.

A) Root growth response to IAA (10 nM) for 20 minutes, 1 hr, 3hr and 6hr. Root growth response represents growth in treatment normalized to the respective mock condition.

B) Root growth response of Col-0, *afb1*, *tir1afb2*, and *tir1afb345* seedlings to IAA (10nM; 15 min)

C) Gravitropic response of Col-0, *afb1*, *tir1afb2*, and *tir1afb345* roots. Mean root tip angle ± s.d. (error bars), time after a 90° gravistimulation is indicated, n=10–14 individual roots.

D) Schematics of ccvAFB1 receptor design. Highlighted amino acid is the substitution in TIR1 and AFB1 that confers cvxIAA binding.

E) In vitro pull-down assays of ccvAFB1-mScarlet by IAA7-DII peptide co-incubated with mock (m) 10 μM cvxIAA or 10 μM IAA. Input is shown (IN), ccvAFB1-mScarlet detected by anti-mCherry antibody. MW of ccvAFB1-mScarlet = 92 kD. Full membrane is shown in Fig.S4.

F) Subcellular localization of *ccvAFB1-mScarlet* and *ccvTIR1-mScarlet* (green) in Arabidopsis root tips counterstained with propidium iodide (magenta); both constructs controlled by *pTIR1* promoter. Scale bars = 50 μm.

G) Root growth of Col-0, *afb1–3*, and *ccvAFB1* (*afb1–3*) after 15-minute treatment with mock, IAA (10 nM), cvxIAA (500 nM) or their combination Only *ccvAFB1* roots respond to cvxIAA.

Boxplots in A, B, G represent the median and the first and third quartiles, and the whiskers extend to minimum and maximum value; all data points are shown as dots. Statistical difference according to Ordinary one-way ANOVA coupled with Tukey's multiple comparison tests ($p<0.05$) indicated by letters.

H) A kymograph showing auxin-induced R-GECO1 intensity increase indicating cytosolic calcium ($[Ca^{2+}]_{cyt}$) transients after application of 150 nM IAA (arrow) in Col-0 and *afb1–3* root epidermal cells. Fluorescence intensity look-up table is indicated. I-K) Quantification of calcium ($[Ca^{2+}]_{cyt}$) in response to auxin treatment. I) Response of Col-0 and *afb1–3* root epidermal cells to 150 nM IAA. J) Response of *ccvAFB1-mVenus*, *ccvTIR1-mScarlet* and Col-0 root epidermal cells to 500 nM cvxIAA. K) Response of *tir1afb2* root epidermal cells to 150 nM IAA, shown with positive (Col-0) and negative control (*afb1–3*). I-K) Normalized mean R-GECO1 fluorescence intensity F/F_0 ± s.d. (represented as shaded areas). Auxin treatment is indicated by arrows.

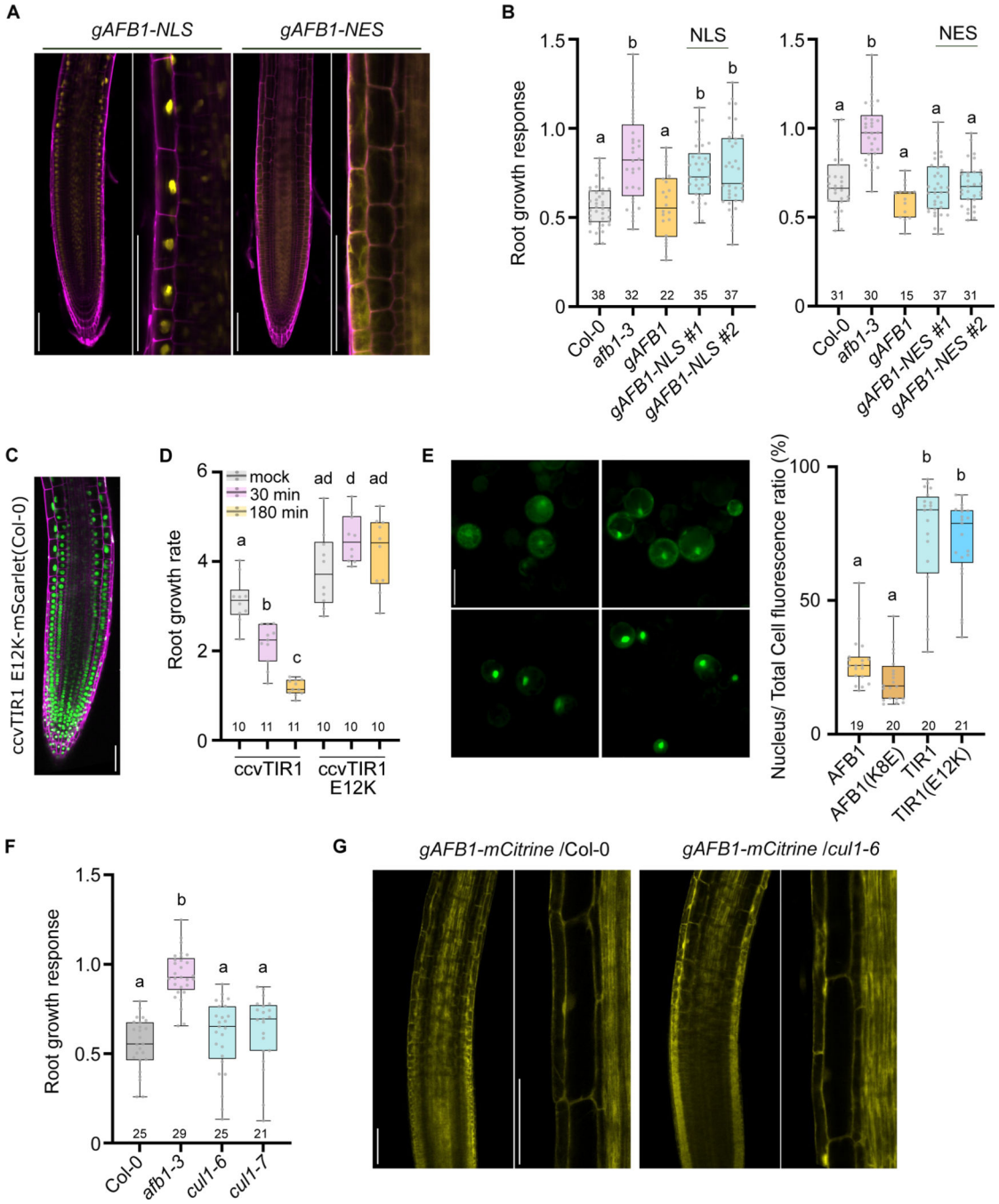

Figure 2: Cytoplasmic AFB1 regulates rapid root growth.

A) Subcellular localization of AFB1-NLS-mCitrine and AFB1-NES-mCitrine (yellow) in *afb1–3*; roots stained with propidium iodide (magenta). Scale bars = 100 μm.

B) Root growth response (growth of treated roots normalized to growth of the respective mock-treated roots) of Col-0, *afb1–3*, *gAFB1* (*afb1–3*) and *gAFB1-NLS/NES #1, #2* (*afb1–3*) to IAA (10 nM; 20 minutes).

C) The ccvTIR1-E12K-mScarlet (Col-0) protein (green) localizes to nuclei. Stained with propidium iodide (magenta), scale bar = 50 μm.

D) Root growth rate of *ccvTIR1-mScarlet* (Col-0) and *ccvTIR1-E12K-mScarlet* (Col-0) in mock or 500 nM cvxIAA treated seedlings.
E) Subcellular localization of AFB1, AFB1(K8E), TIR1, and TIR1(E12K)-GFP in Col-0 *Arabidopsis* protoplasts (left) and quantification of relative nuclear localization (right), calculated as the ratio of nuclear fluorescence to total cell fluorescence.
Scale bar = 50 μm.
F) Root growth response of Col-0, *afb1–3*, *cul1–6* and *cul1–7* to IAA (10 nM; 20 minutes).
G) Expression pattern and subcellular localization of AFB1-mCitrine in Col-0 and *cul1–6* background. Scale bar = 100 μm. Boxplots in B,D,E,F represent the median and the first and third quartiles, and the whiskers extend to minimum and maximum value; all data points are shown as dots. Letters indicate statistical differences according to Ordinary one-way ANOVA coupled with Tukey's multiple comparison tests ($p<0.05$).

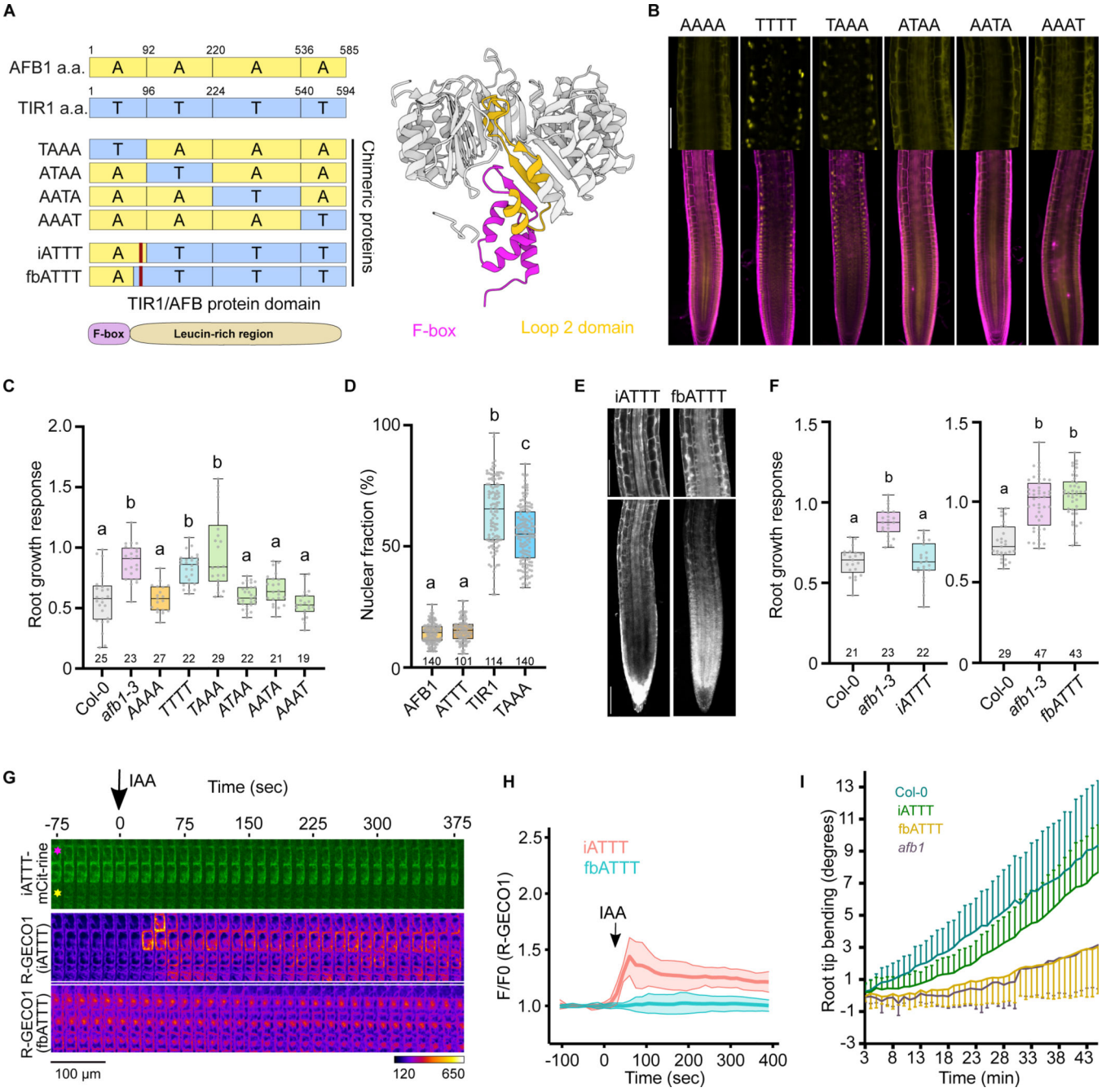

Figure 3: The N- terminal region of AFB1 is crucial for its role in the rapid auxin response.

A) Schematic diagram of domain swap AFB1 (A-yellow) and TIR1 (T-blue) constructs. Numbers indicate amino acid position. Chimeric iATTT protein contains the F-box domain (magenta in 3D structure) and adjacent sequences in the LRR region (yellow in 3D structure) from AFB1, while the chimeric fbATTT protein contains only the AFB1 F-box domain (magenta in 3D).

B) Expression pattern and subcellular localization of AFB1 (AAAA), TIR1 (TTTT) and chimeric proteins (TAAA, ATAA, AATA, AAAT). All domain swap proteins were regulated

by the *AFB1* promoter in the *afb1–3* background. Scale bar = 100 μm, stained with propidium iodide (magenta).

C) Root growth response of Col-0, *afb1–3*, and domain swap lines to IAA (10 nM, 20 minutes); growth of treated roots normalized to growth of the respective mock-treated roots.

D) Quantification of nuclear fraction of fluorescence signal of the AFB1-mCitrine, ATTT-mCitrine, TIR1-mCitrine, TAAA-mCitrine Arabidopsis lines; see Fig. S2B,E) Expression pattern and subcellular localization of iATTT-mCitrine and fbATTT-mScarlet proteins. The iATTT and fbATTT proteins were regulated by the *AFB1* and *TIR1* promoters respectively in the *afb1-3* background. Scale bar=100 μm.

F) Root growth response of Col-0, *afb1–3*, *iATTT* (*afb1–3*) and *fbATTT* (*afb1–3*) roots to IAA (10 nM) for 20 minutes.

G) A kymograph showing auxin-induced cytosolic Ca^{2+} transients (R-GECO1 intensity) during application of 150 nM IAA (arrow) in iATTT(*afb1*) and fbATTT(*afb1*) root epidermal cells. On the top, the iATTT-mCitrine channel highlights the patchy expression of the construct, note that the iATTT-expressing cell (magenta asterisk) also shows higher Ca^{2+} transient than the weakly-expressing cell (yellow asterisk). Fluorescence intensity look-up table is indicated.

H) Quantification of R-GECO1 intensity indicating $[Ca^{2+}]_{cyt}$ transients in iATTT and fbATTT root epidermal cells. IAA treatment (150 nM) shown by an arrow. n = 6–11 Boxplots in C, E represent the median and the first and third quartiles, and the whiskers extend to minimum and maximum value; all data points are shown as dots.

I) Quantification of the gravitropic response in Col-0 (n=20), *afb1* (n=12), *iATTT* (n=23), and *fbATTT* (n=23) roots. Mean root tip angle ± s.d. (represented as error bars) is shown. Time after 90° gravistimulation is indicated.

Boxplots in C, D, F represent the median and the first and third quartiles, and the whiskers extend to minimum and maximum value; all data points are shown as dots. Letters indicate statistically different groups according to Ordinary one-way ANOVA coupled with Tukey's multiple comparison tests ($p<0.05$).

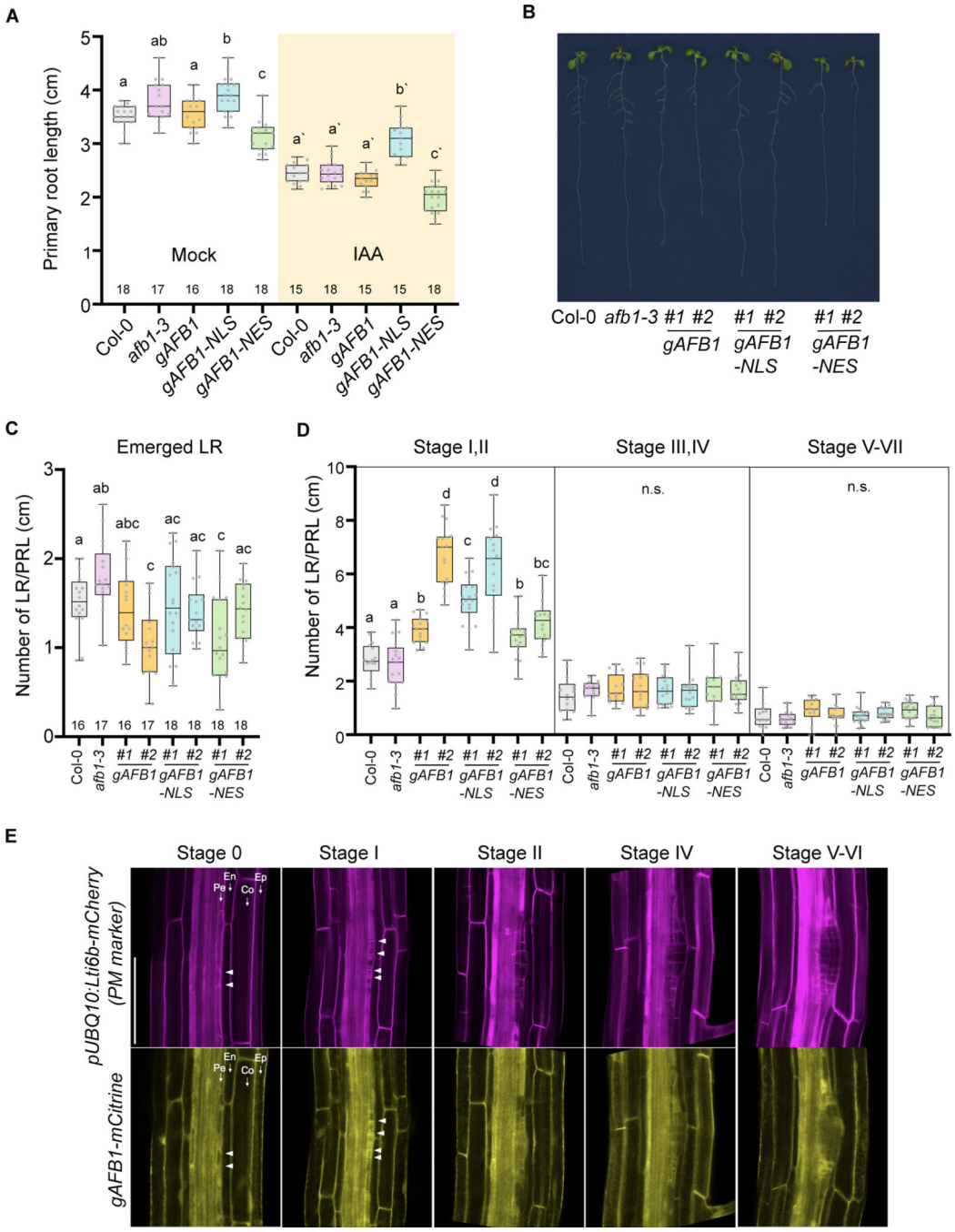

Figure 4: AFB1 negatively regulates canonical auxin signaling.

A) Primary root length of five-day-old seedlings of Col-0, *afb1–3*, *gAFB1* (*afb1–3*), and *gAFB1-NLS/NES* (*afb1–3*) lines treated with either 100 nM IAA or mock (ethanol) for 3 days.

B) Lateral root phenotype in nine-day-old seedlings of Col-0, *afb1–3*, *gAFB1* (*afb1–3*), and *gAFB1-NLS/NES* (*afb1–3*) lines.

C) Number of emerged lateral roots per primary root length in Col-0, *afb1–3*, *gAFB1* (*afb1–3*) and *gAFB1-NLS/NES* (*afb1–3*) lines (#1 and #2 indicates two independent lines).

D) Number of non-emerged primordia at different stages in lateral root developed expressed per primary root length in Col0, *afb1–3*, *gAFB1* (*afb1–3*) and *gAFB1-NLS/NES* (*afb1–3*) lines (#1 and #2 indicates two independent lines).
E) Expression pattern of gAFB1-mCitrine; pUBQ10:Lti6b-mCherry during lateral root development. pUBQ10:Lti6b-mCherry was used as a plasma membrane marker. Ep; Epidermis, Co; Cortex, En; Endodermis, Pe; Pericycle. Scale bar = 100 μm.
Box plots represent the median and the first and third quartiles, and the whiskers extend to minimum and maximum value; all data points are shown as dots. Letters above box plots indicate statistical differences according to Ordinary one-way ANOVA coupled with Tukey's multiple comparison tests ($p<0.05$).